Publication V

Manuscript reprinted from International Journal of Energy Research (in press)

Estimating thermal stress in BIPV modules

Petri Konttinen, Thomas Carlsson, Peter Lund, Teijo Lehtinen

Nomenclature

A	PV module area (m^2)
a	fraction of solar energy absorbed in PV module
C	heat capacitance (J/K)
D	constant in Arrhenius equation
E	energy (in Arrhenius equation)
G	plane-of-array irradiance (W/m^2)
h	convective heat transfer coefficient (W/m^2K)
k	thermal conductivity (W/mK), (Boltzmann's) constant (J/K)
L	thickness (m)
P	performance
q	heat transfer rate (W)
r	degradation rate
T	temperature (K)
t	time

Greek

ε	emittance
η	PV module electrical efficiency
γ	fraction of one year
σ	Stefan-Boltzmann's constant (W/m^2K^4)
τ	module lifetime

Subscripts

0	beginning of iteration calculation
1	node
3	node
a	activation (in Arrhenius equation)
A	accelerated
air	airgap
amb	ambient
B	Boltzmann's
cap	capacitive heat sink
g	glass, façade glass and silicone assembly
hi	heat capacity (at node i)
i	insulator, node, relation between time (t) and temperature (T)
j	node
k	time step, iteration step
m	iteration step
mod	PV module
N	normal operating conditions

Summary

The thermal stress on building-integrated photovoltaic modules (BIPV) in Espoo, Finland, was studied with field-testing of amorphous silicon modules. Based on these results, the thermal stress at two other European locations (Paris and Lisbon) was estimated. The estimation procedure entailed thermal modeling of heat transfer in the facade with meteorological data as input. The results indicate that the thermal stress on BIPV modules in Lisbon is in this case approximately 50 % higher that in Espoo and between 80 – 200 % higher than in Paris, depending on the activation energy of the degradation process. The difference in stress between a BIPV module and a free-standing module in Espoo was 50 – 200%.

Keywords: BIPV, amorphous silicon, photovoltaic, lifetime, stability, temperature, thermal modeling

1. Introduction

Photovoltaic (PV) modules are used throughout the world in varying operating conditions. They must withstand high and low temperatures, short term temperature cycles, rain, ice and UV-light. In addition, modules often operate in arrays, where the voltage between module and frame can be several hundred volts. PV modules need to be resistant enough to these stress factors to maintain their power output at a steady level for at least 20-30 years. High reliability is a key factor in increasing the amount of electricity a module is expected to produce which is equivalent to decreasing PV electricity price.

A key challenge for PV technologies is the estimation of module lifetime. The basic estimation approach centers on the use of accelerated aging tests with suitable stress factors to simulate a given number of years in field operation. Stress factors need to be selected carefully since they should reproduce performance degradation mechanisms which occur in field operation without producing additional aging in the module through mechanisms which are not relevant in the field (Czanderna and Jorgensen, 1999). High degrees of uncertainty enter lifetime predictions if stress factors pertinent to one PV technology are applied indiscriminately to other technologies or when the calculated lifetime is assumed to be independent of geographical location. In normal operation, high temperatures and temperature cycles can be considered the most important stress factors affecting PV module performance.

The importance of high temperature is due to the large number of degradation effects whose reaction rates are directly determined by temperature. In the active solar cell material, these effects include diffusion of dopants and impurities as well as corrosive reactions at contacts and interfaces (McMahon, 2004). Many degradation mechanisms which occur in the encapsulant polymer protecting the active material, such as the

penetration of moisture or photothermal reactions which weaken the adhesive and optical properties of the polymer, are also thermally driven (Czanderna and Pern, 1996; Allen et al., 2001; Pern and Glick, 2000). In many of these cases the effect of temperature on performance degradation can be adequately modeled with the help of the Arrhenius relation between reaction rate and temperature, and accelerated aging tests can be used to study the temperature-dependence of degradation mechanisms in detail in the laboratory. Extending these results to actual operating conditions requires temperature histograms from field test measurements on the module in question. While these can often be measured at some locations, the climate range which real measurements cover is usually limited and there is a significant lack of geographical scope in lifetime predictions for PV modules today.

A number of studies have been published on long-term field testing of a-Si thin-film photovoltaic modules (Hahn et al., 1990; Akhmad et al., 1997; del Cueto and McMahon, 2000; Rüther et al., 2003). From the perspective of lifetime prediction, the utility of basic field measurements is limited unless some information on the degradation mechanisms responsible for performance changes in the module can also be gained. In some cases, such as the Staebler-Wronski effect in a-Si modules (Staebler and Wronski, 1977), field measurements can be interpreted as direct evidence of a particular degradation mechanism at work (Hahn et al., 1990; Akhmad et al., 1997; Rüther et al., 2003).

A large proportion of photovoltaic installations today are building integrated. This approach has several advantages: there is no need for extra land for the PV system, mounting costs can be reduced and cladding or roofing material replaced with the PV, and the system can be an architectural part of the building concept. However, building integration affects PV module temperature due to limited cooling compared to a free standing PV system. Higher operating temperature has a negative effect both to the efficiency and lifetime of the PV system. The effect of high temperature on efficiency varies between different PV technologies. Amorphous silicon (a-Si) may be a good choice of PV technology compared to crystal-Si for operation in warm and sunny climates (Akhmad et al., 1997) especially for building-integrated photovoltaic (BIPV) systems (Rüther et al., 2003). Still, for any PV technology higher operating temperatures due to building integration causes higher temperature-induced degradation during the lifetime of the system.

In this paper, a heat-transfer model for BIPV modules is used to estimate the dependence of module temperature on plane-of-array irradiance and ambient temperature. The model is checked by comparing the temperature histogram obtained from actual temperature measurements to the histogram predicted by the model. Meteorological data from Paris and Lisbon is then used to compare the thermal stress which the modules would be exposed to in identical façades at those locations. This gives a general framework for estimating the temperature-limited lifetime of the modules at these locations when the specifics of relevant temperature-dependent degradation mechanisms are known from accelerated aging tests in the laboratory. The greater availability of meteorological data compared to PV module temperature data makes this approach much more widely applicable than those based on measured temperature histograms. The methodology proposed here thus addresses climatic variation as a factor influencing the lifetime of PV modules.

2. Methods

2.1 Temperature measurements with a-Si modules

Module temperatures (T_{mod}) were measured from amorphous silicon (a-Si) photovoltaic modules installed at the Helsinki University of Technology solar energy testsite in Espoo, Finland (60°11' N, 24°49' E). Figure 1 shows the vertical array of six single-junction a-Si systems in a retrofit PV façade installed southwards on the side of a wooden container. The systems were separated by the white battens shown in Figure 1.

Figure 1*. Vertical array of six single-junction a-Si modules in a retrofit BIPV façade installed southwards on the side of a wooden container in Espoo, Finland. Locations of temperature sensors a-g are shown.*

Each system included three modules, separated by the black area. Figure 2 shows a vertical cross section of the façade, with numbered nodes for the heat transfer calculations. T_{mod} was measured at seven points marked with the letters a…g in Figure 1. Temperature sensors a-d were laminated between the PV glass and the back glass, and sensors e-g behind the back glass. All the T_{amb} sensors were of PT100 –type according to DIN IEC 751 class B. The BIPV façade was manufactured for the Joule-Thermie Project ASICOM (Lund *et al*., 1999).

Figure 3 shows four triple-junction a-Si modules installed on a free-standing metal roof tilted southwards at angle of 45^{o}. These modules are Uni-Solar 64 W_p PV-laminates attached with a butyl adhesive to a black painted metal roof. The metal roof is of a standard type manufactured by Rannila, a subsidiary of Ruukki. Module temperatures, plane-of-array irradiance (G) and ambient temperature (T_{amb}) were measured from the BIPV façade every 5 minutes from September 1998 to May 2001. For the free-standing façade, T_{mod} and G were measured every 30 minutes from March 2002 to September 2004.

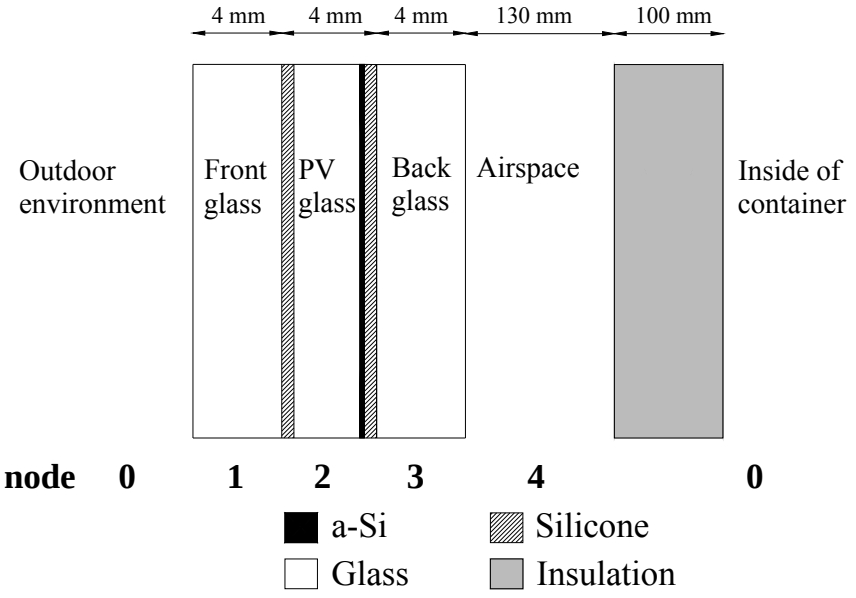

Figure 2. *Cross-section of vertical BIPV façade, with heat transfer calculation nodes numbered. Node 2 includes the PV material, the PV glass and the silicone layers.*

Figure 3*. Four triple-junction a-Si modules installed on a free-standing metal roof tilted southwards at angle of 45^{o}. The module type is Uni-Solar 64 W_p PV-laminate with a butyl adhesive, and they are attached to a standard black painted metal roof manufactured by Ruukki.*

2.2 Heat transfer modeling of a BIPV façade

Since meteorological data is usually available from a much larger number of different locations than PV module temperature data, it is useful to develop models for predicting module temperature from basic meteorological variables. In the case of BIPV modules, the temperatures can be estimated by solving heat transfer equations which describe the thermal fluxes arising in the BIPV structure when exposed to given values of G and T_{amb}. As seen in Figure 2, the façade consisted of a 4mm thick front glass, a 4mm thick photovoltaic module glass protected by a thin layer of silicone gel on both sides with the a-Si PV material deposited on the back side, a 4mm thick back glass, an open airspace of 130mm width and a 100mm thick back insulation.

In the modeling of heat transfer within this system, heat fluxes were calculated between four different nodes numbered in Figure 2: 1) front glass 2) PV module 3) back glass and 4) airspace. Nodes labeled with zero are included for notation purposes and indicate the ambient conditions surrounding the container. For the purpose of this model, the PV module (including silicone layers) was assumed to act as a single component from a heat transfer perspective, and a 4mm thick glass barrier was assumed between nodes 1–2 and 2–3. All of the incident sunlight was assumed to be absorbed in node 2, the insulator surface temperature was assumed to be equal to the air temperature in the airspace and the inside of the ventilated container was assumed to be at outdoor ambient temperature.

The following system of equations describes heat transfer in the modeled vertical façade system, with heat transfer rates denoted by q. Heat transfer rate subscripts indicate the source and target nodes (Figure 2), respectively, and the chosen sign convention is $q > 0$ for heat transfer to the node and $q < 0$ for transfer away from the node. At node 1, heat is transferred between the environment and the glass radiatively and convectively (Eq. 1), and between the PV module and the glass by conduction (Eq. 2).

$$q_{01} = \left[\varepsilon_g \cdot \sigma \cdot \left(T_{sky}{}^4 - T_1{}^4\right) + \left(T_{amb} - T_1\right) \cdot \bar{h}_w\right] \cdot A \quad (1)$$

$$q_{12} = \left(T_{mod} - T_1\right) \cdot k_g \cdot \frac{1}{L_g} \cdot A \quad (2)$$

where ε_g is the emittance of the glass, σ is the Stefan-Boltzmann constant, T_{amb} is the ambient temperature, T_{sky} is the sky temperature calculated as $T_{amb} - 5K$, T_1 is the temperature at node 1 and A is the PV module area. The average wind convection coefficient is $\bar{h}_w$, the thermal conductivity of the glass-silicone assembly is k_g and L_g is the glass thickness. At node 2, the heat transfer fluxes are conduction to/from the front and back glasses (Eqs. 2 and 3) and the solar energy flux which is absorbed by the PV module but not converted to electricity (Eq 4).

$$q_{23} = (T_3 - T_{mod}) \cdot k_g \cdot \frac{1}{L_g} \cdot A \tag{3}$$

$$q_{02} = G \cdot a \cdot (1 - \eta) \cdot A \tag{4}$$

where T_3 is the temperature of the back glass, a is the fraction of solar energy absorbed in the module and η is the electrical efficiency of the module. Node 3 is affected by convection from the module (Eq. 3) and radiative and convective (Eq. 5) heat transfer to/from the airspace.

$$q_{34} = \left[\sigma \cdot \left({T_{air}}^4 - {T_3}^4 \right) \cdot \frac{1}{\frac{1}{\varepsilon_g} + \frac{1}{\varepsilon_i} - 1} + (T_{air} - T_3) \cdot h_{air} \right] \cdot A \tag{5}$$

where T_{air} is the temperature in the airspace (and the temperature of the inner insulator surface), ε_i is the emittance of the insulator and h_{air} is the convection coefficient in the air space. At node 4, the components are radiative and convective heat transfer (Eq. 5), heat conduction through the back insulation and ventilation heat loss (both in Eq. 6).

$$q_{40} = (T_{amb} - T_{air}) \cdot \left[k_i \cdot \frac{1}{L_i} \cdot A + \rho_{air} C_{air} \dot{V}_{air} \right] \tag{6}$$

where k_i is the thermal conductivity of the insulation and L_i is the insulator thickness. Ventilation heat loss is determined by the rate of air volume exchange $\dot{V}_{air}$, air density ρ_{air} and air heat capacity C_{air}. The product of these three terms was estimated to be 0.10 W/K for the BIPV façade studied here. Finally, a capacitive heat sink component was added to each node 1-4 to take into account its thermal mass. It was of the form

$$q_{cap} = C_{hi} \frac{(T_i(t_m) - T_i(t_k))}{t_k - t_m} \tag{7}$$

where q_{cap} is the capacitive heat transfer rate, C_{hi} is the heat capacitance at node i and T_i is the temperature at node i. The variables t_m and t_k (with $t_k > t_m$) indicate consecutive time steps.

The set of equations 1–7 was solved for meteorological data containing time series of G and T_{amb}. At a given time step t_k the temperatures at each node were solved by imposing the condition $\Sigma q = 0$ on each node and iteratively finding the node temperatures consistent with the irradiance G_k, the ambient temperature $T_{amb,k}$ and the node temperatures calculated in the previous step. The numerical values of parameters in equations 1–7 are given in Table 1. Values which are approximations are indicated with an asterisk.

Table 1. Numerical values used in equations 1–7.

Parameter	Value	Unit
ε_g	0.9*	-
ε_i	0.9*	-
k_g	0.53*	W/mK
k_i	0.037	W/mK
L_g	0.004	m
L_i	0.1	m
$\overline{h}_w$	5.8	W/m^2K
h_{air}	1.9	W/m^2K
A	1.27	m^2
η	0.03	-
a	0.99	-

* = approximate value

2.3. Modeling of temperature-dependent degradation mechanisms

Accelerated aging experiments are based on the calculation of an acceleration factor which relates the lifetime in normal operating conditions, τ_N, to lifetime in the accelerated aging experiment, τ_A. In most cases, the lifetime of a PV module is considered to end when its performance drops below a certain level defined as the failure point. When the stress factor is high temperature, the degradation reaction rate often follows the Arrhenius temperature dependence. If the performance is assumed to depend linearly on how far the degradation reaction has proceeded, the drop in performance after time t since the beginning of the aging experiment (conducted at constant temperature T) is written as

$$\Delta P(T,t) = r(T) \cdot t = D \cdot \exp(-E_a/k_B T) \cdot t \quad (8)$$

where ΔP is the performance drop, r is the rate of degradation, D is a constant which can be experimentally determined, E_a is the activation energy of the degradation mechanism and k_B is Boltzmann's constant. In PV modules, the degradation reactions which can be expected to show Arrhenius behaviour include the diffusion of impurities and dopants in the solar cell material, the diffusion of moisture and contaminates in the encapsulant and thermal oxidation of the cell or encapsulant. In real operating conditions, modules

experience a number of different operating temperatures, and the performance drop at τ_N can then be written as

$$\Delta P(\tau_N) = \sum_i r(T_i) \cdot t_i = \sum_i D \cdot \exp(-E_a/k_B T_i) \cdot t_i \quad (9)$$

where t_i is the time the PV module has spent at temperature T_i. This time can be written as $t_i = \gamma_i \tau_N$, where γ_i is the fraction of one year which the module spends at temperature T_i. If we assume that both E_a and the failure point are independent of temperature, the latter condition being $\Delta P(\tau_N) = \Delta P(T_i,\tau_i)$ where τ_i is module lifetime at the constant temperature T_i, the lifetime in normal operating conditions can be written as

$$\tau_N = \frac{1}{\sum_i \frac{\gamma_i}{\tau_i}} = \frac{\tau_A}{\sum_i \gamma_i \cdot \exp\left[E_a \left(\frac{1}{k_B T_A} - \frac{1}{k_B T_i} \right) \right]} \quad (10)$$

where τ_A now refers to module lifetime in an accelerated aging experiment where the stress factor is the constant temperature T_A. It is evident that module temperature histograms spanning one representative year are sufficient for calculation of the acceleration factor in Eq. (10).

3. Results and discussion

3.1. Measured and modeled temperatures and histograms

One hour average values were calculated from the measured BIPV façade module temperatures (T_{mod}) (see Figure 1). On days with high irradiance, a typical average standard deviation in T_{mod} for the sensors a-d laminated in between the glass panes was in the range of 0.4 °C, which was within the measurement error. For the sensors e-g laminated behind the back glass, the typical standard deviation was somewhat higher (~ 0.7 °C), as were the temperature differences between these two sensor sets. The hottest and lowest temperatures were measured for sensors b and a for the in-between sensors, and for sensors g and e for the backside sensors, respectively. Typical temperature behaviour for a high irradiance day is shown in Figure 4.

Average one hour temperatures of all the T_{mod} sensors a-g was used as an estimate for module temperature in the façade. This may have caused slight underestimating of the aging effect for these modules. However, since the measured temperatures represent the middle module column, the maximum temperatures of the left and right modules columns have most probably been lower due to edge heat losses. Measured one year temperature histograms for the BIPV façade and the free-standing roof are shown in Figure 5.

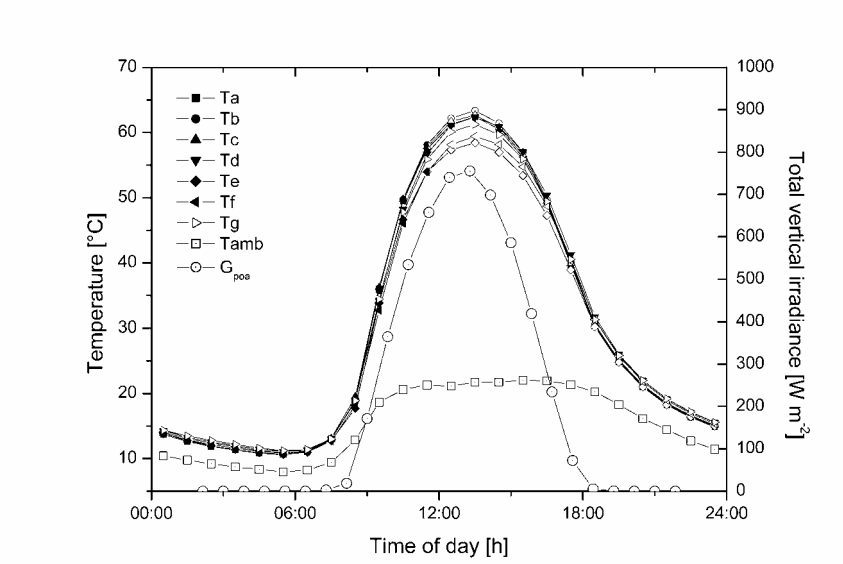

Figure 4. *Typical temperature distribution of the BIPV façade on a high irradiance day. Ta-Tg represents temperature T_{mod} sensors a-g, T_{amb} is measured ambient temperature and G_{poa} is total vertical irradiance on the façade.*

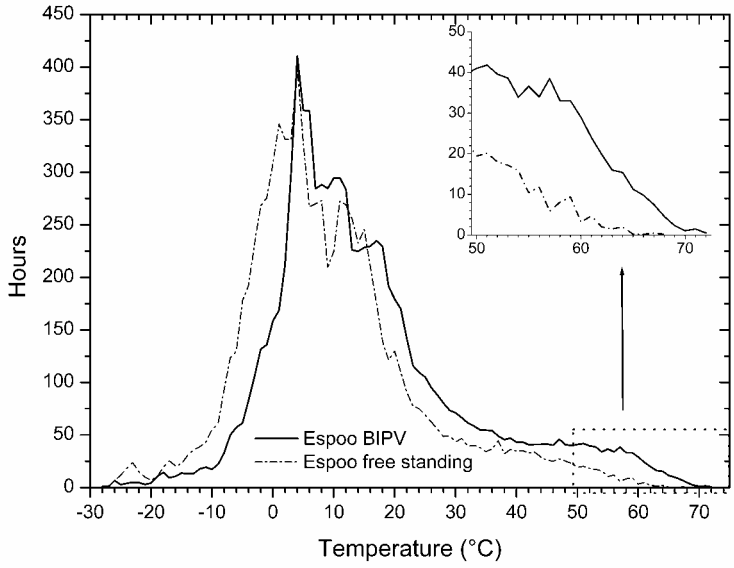

Figure 5. *Measured yearly temperature histograms for the BIPV façade (Figure 1) and the free-standing roof (Figure 3). In the histograms each temperature interval is 1°C wide.*

In the histograms each temperature interval is 1°C wide. The histograms show that the yearly temperature distribution of the free-standing 45° tilt angle roof with a properly ventilated background is at a significantly lower level compared to that of the vertical BIPV façade. Comparison of measured and modeled temperatures for the BIPV façade in Espoo are shown in Figure 6 between 30°C and 75°C. Below 30°C the model is biased to underestimate the temperature to some extent. The error estimate due to this is discussed where modeled data has been used.

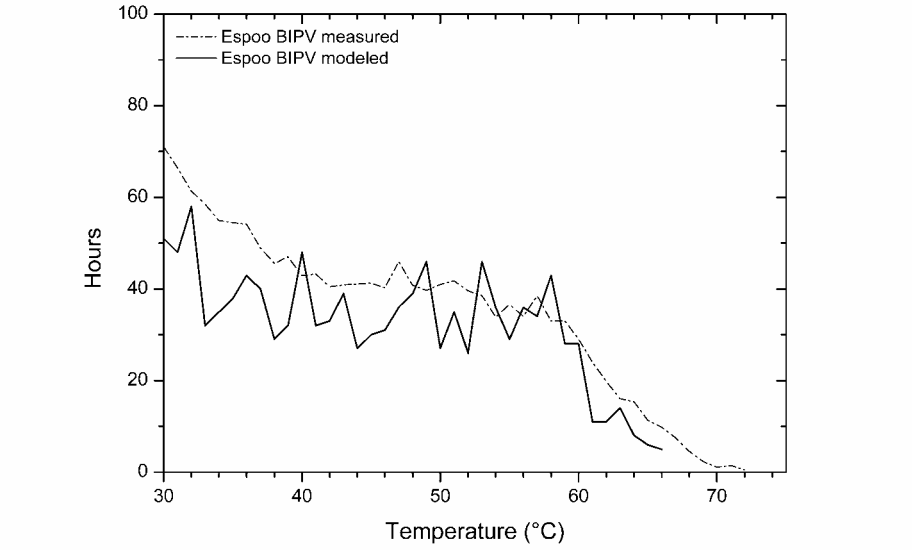

Figure 6. *Measured and modeled yearly temperatures for the BIPV façade between 30°C and 75 °C, each temperature interval being 1°C wide. Above 30°C the modeled data corresponds relatively well with the measured. The model is sensitive to wind speed which explains most of the difference.*

The heat-transfer model used in this work achieved satisfactory results despite its approximations. Modeled and measured temperature histograms in Figure 6 corresponded well to each other at temperatures above 30°C. At lower temperatures, the model predicted lower temperatures than measured. Modeling inaccuracies may be due to node 2, which should possibly be divided into several nodes to obtain a better description of the system. In addition, real wind measurements at a suitable height were not available for Lisbon and Paris, so the assumption that wind conditions were equal everywhere had to be made. In assessing thermal stress, the high-temperature data is most significant, and the calculations performed in this work indicate that the stress can be markedly different in southern and northern European locations, depending not only on sunlight hours but also on façade orientation and tilt angle. This should be taken into account when accelerated aging tests are interpreted. Thermal cycling due to high daily temperature differences may also cause significant stress to BIPV modules. Stress due to temperature cycling has not been included in the model.

3.2 Prediction of thermal stress at various European locations

As an example of using heat transfer models to predict thermal stress in different locations, reference year meteorological data for Paris (48°48' N) and Lisbon (38°44' N) was used to predict the temperature histograms which the modules of the studied BIPV façade would be exposed to at these locations in a vertical southward installation. The reference year data contained hourly averages of global (G_H) and diffuse (G_D) horizontal irradiance and T_{amb}. Approximate values for the G values on a vertical installation were calculated from the available G_H and G_D data by standard methods. The temperature histograms predicted by the model are presented in Figure 7, each temperature interval being 1°C wide. It can be seen that the modules in the façade at Lisbon are predicted to spend significantly more time at temperatures above 40°C than the ones at the other locations. The Paris data has less cumulative time at temperatures above 60°C than the measured histogram data from Espoo, shown in Figure 5. The latter phenomenon is likely to be due to the larger solar zenith angle in Espoo which gives more sunlight on a vertical installation in the summer. This is an important effect, since the thermal stress is to a large extent determined by the high-temperature end of the histogram.

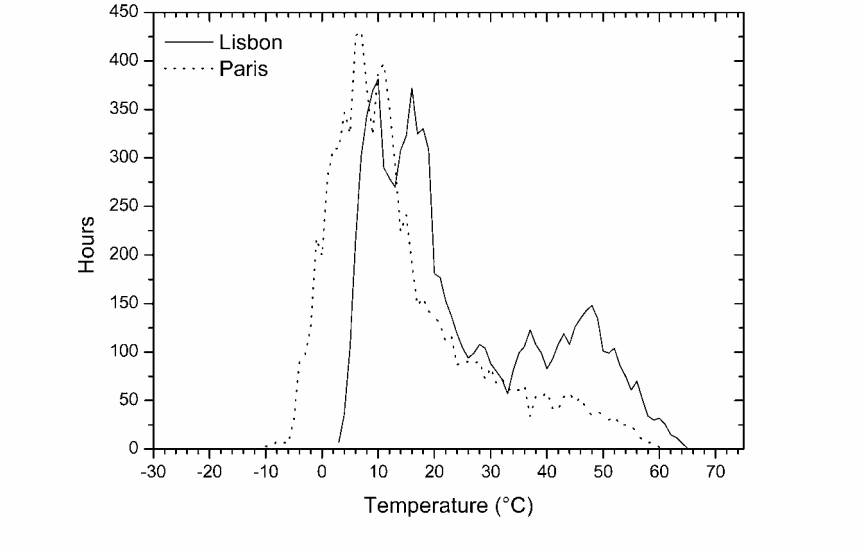

Figure 7. *Yearly temperature histograms predicted by the model for the BIPV facade in Paris and Lisbon, each temperature interval being 1°C wide.*

To elucidate the effect of differences in temperature histograms on thermal stress, the acceleration factors at different accelerated aging temperatures T_A were calculated according to Eq. (3) from the histogram data in Figures 5 and 7 for each location. The temperature dependence of the acceleration factors is illustrated in Figure 8, where the

stress time needed to simulate 30 years of outdoor operation at the given location is plotted against the stress temperature T_A for two different activation energies. The lower activation energy E_a = 0.4 eV applies to the diffusion of water in the commonly used encapsulant polymer EVA (Kempe, 2005), while E_a = 1.0 eV is taken as an upper limit for relevant degradation mechanisms. For both activation energies, the time required to simulate 30 years of operation at Lisbon is approximately one and a half times as long as the corresponding time for the BIPV installation in Espoo. Although the curves for Espoo BIPV and Paris nearly overlap for E_a = 0.4 eV, in the case of E_a = 1.0 eV the curve from Paris lies significantly lower than that of Espoo. This illustrates how the higher activation energy magnifies the effect of the high temperature histogram data shown in Figure 7. For a comparison between free-standing and BIPV applications, the stress curve for the free-standing façade shown is also shown in Figure 8. It can be seen that the time needed to simulate 30 years of outdoor operation in Espoo for the free-standing modules is in the case of E_a = 0.4 eV approximately 70 % of the time needed for the BIPV application, and for E_a = 1.0 eV only about 30 % of it.

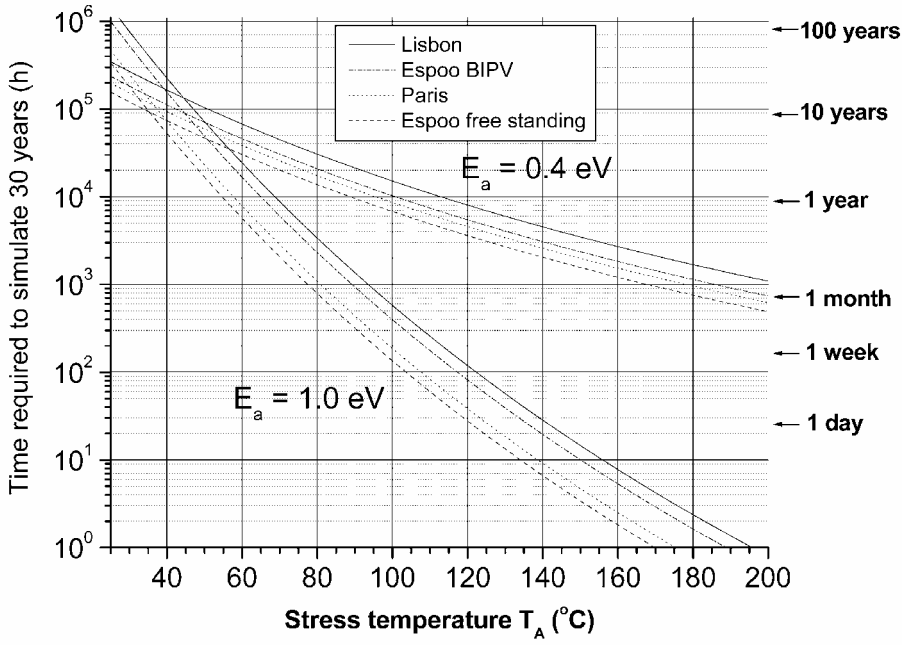

Figure 8. *Temperature dependence of the acceleration factors, where the stress time needed to simulate 30 years of outdoor operation at the given location is plotted against T_A for two different activation energies. Curves were calculated from the histogram data in Figures 5 and 7. Approximate error estimates for modeled curves (Paris and Lisbon) are 17% for E_a = 0.4 eV and 25% for E_a=1.0 eV.*

4. Conclusions

This paper presents a methodology for estimating module temperatures in BIPV systems from meteorological data. It is based on thermal modeling of a BIPV façade, which allows module temperature to be calculated from irradiance and ambient temperature data. This method can be used to assess the thermal stress on the BIPV modules in different climates. A connection can then be made between lifetime in thermal accelerated tests and field lifetime if the activation energy related to a given performance-limiting degradation mechanism is known. In the example considered in this paper, the performance drop was assumed to depend linearly on how far the degradation process has proceeded. More complicated relationships between degradation reactions and performance loss can be used as needed.

The results presented for the BIPV façade and the free-standing roof give an indication of the large difference in thermal stress between the two installations. These results are not perfectly comparable due to differences in tilt angle, module type and encapsulation method, but they nevertheless give an approximate idea of the difference. In conclusion, thermal modeling of BIPV façades is a simple and versatile tool for addressing the lack of PV module field-test data from multiple locations in different climates. The significant differences between thermal stress at different locations illustrate the need for using temperature histograms from a number of different locations when PV module lifetime is estimated.

The results indicate that the thermal stress on BIPV modules in Lisbon is in this case approximately 50 % higher that in Espoo and between 80 % and 200 % higher than in Paris, depending on the activation energy of the degradation process. The difference in stress between a BIPV module and a free-standing module in Espoo was estimated to be between 50 % and 200 %, depending on the activation energy.

References

Akhmad K, Kitamura A, Yamamoto F, Okamoto H, Takakura H, Hamakawa Y. 1997. Outdoor performance of amorphous silicon and polycrystalline silicon PV modules. *Solar Energy Materials & Solar Cells* **46**(3): 209-218. DOI: 10.1016/S0927-0248(97)00003-2.

Allen N, Edge M, Rodriguez M, Liauw C, Fontan E. 2001. Aspects of the thermal oxidation, yellowing and stabilisation of ethylene vinyl acetate copolymer. *Polymer Degradation and Stability* **71**(1): 1-14. DOI: 10.1016/S0141-3910(00)00111-7.

Czanderna A, Pern F. 1996. Encapsulation of PV modules using ethylene vinyl acetate copolymer as a pottant: A critical review. *Solar Energy Materials & Solar Cells* **43**(2): 101-181. DOI: 10.1016/0927-0248(95)00150-6

Czanderna A, Jorgensen G. 1999. Accelerated life testing and service lifetime prediction for PV technologies in the twenty-first century. *Electrochemical Society Proceedings 99-11 (Photovoltaics for the 21st century)*. 57-67.

del Cueto J, McMahon T. 2000. Performance of Single-Junction a-Si Modules Under Varying Conditions in the Field. *Conference Record of the 26th IEEE PV Specialists Conference*. 1205-1208. DOI: 10.1109/PVSC.1997.654305.

Hahn M, Berry W, Mrig L. 1990. Comparative Short Term / Long Term Field Test Performance and Stability of Tandem and Single Junction a-Si Modules. *Conference Record of the 21st IEEE PV Specialists Conference*. 1057-1061. DOI: 10.1109/PVSC.1990.111779.

Kempe M. 2005. Control of moisture ingress into photovoltaic modules. *Conference Record of the 31st I5 PV Specialists Conference.* 1038-1039.

Lund, P., Vartiainen, E., Ross, M. et al. 1999. EU-JOULE JOR3-CT96-0096 ASICOM Amorphous-Si Photovoltaics for Commercial Buildings, *Final Report to the European Commission, Summary*: Helsinki University of Technology, Advanced Energy Systems, Finland.

McMahon, T. 2004. Accelerated Testing and Failure of Thin-Film PV Modules. *Progress in Photovoltaics.* **12** (2-3)**:** 235-248. DOI: 10.1002/pip.526.

Pern F, Glick S. 2000. Photothermal stability of encapsulated Si solar cells and encapsulation materials upon accelerated exposures. *Solar Energy Materials & Solar Cells* 61(2): 153-188. DOI: 10.1016/S0927-0248(99)00108-7.

Rüther R, Knob P, Beyer H G, Dacoregio M M, Montenegro A A. 2003. High performance ratios of a double-junction a-Si BIPV grid-connected installation after five years of continuous operation in Brazil, *Photovoltaic Energy Conversion, Proceedings of 3rd World Conference on Volume 3.* 2169 – 2172. DOI: 10.1109/WCPEC.2003.1305014.

Staebler D L, Wronski C R. 1977. Reversible conductivity changes in discharge-produced amorphous silicon. *Journal of Applied Physics Letters* **31**(4): 292–294.